Chinese Chemical Letters 34 (2023) 107584

Contents lists available at ScienceDirect

Chinese Chemical Letters

journal homepage: www.elsevier.com/locate/cclet

Heterogeneous photocatalytic borylation of aryl iodides mediated by isoreticular 2D covalent organic frameworks

Pengna Shang[a,1], Xiaoli Yan[a,1], Yang Li[a], Junji Liu[a,*], Guang Zhang[a,*], Long Chen[a,b,*]

[a] Department of Chemistry and Tianjin Key Laboratory of Molecular Optoelectronic Science, Tianjin University, Tianjin 300072, China
[b] State Key Laboratory of Supramolecular Structure and Materials, College of Chemistry, Jilin University, Changchun 130012, China

ARTICLE INFO

Article history:
Received 6 April 2022
Revised 22 May 2022
Accepted 6 June 2022
Available online 10 June 2022

Keywords:
Covalent organic frameworks
Nitrogen-rich
Heterogeneous photocatalysis
Borylation
Green organic synthesis

ABSTRACT

Metal-free heterogeneous photocatalysts provide an environmental-friendly and cost-efficient avenue for green organic synthesis. Covalent organic frameworks (COFs) as heterogeneous photocatalysts showcase promising potential in the field of photocatalytic organic reactions due to their high porosity, insolubility and tailor-made functions. However, thus far, COF-based catalysts only mediated a few types of reactions. Herein, we developed a series of isoreticular nitrogen-rich covalent organic frameworks (N-COFs) with comparable porous structures as photocatalysts which effectively mediated the borylation of aryl iodides with broad substrate scope. Remarkably, 6N-COF exhibits excellent photocatalytic efficiency and superior recyclability. It suggests a new pathway to construct efficient heterogeneous photocatalysts for the borylation of aryl halides.

Covalent organic frameworks (COFs) represent an emerging class of crystalline organic porous materials, which are linked by strong covalent bonds and are mainly composed of light elements, *e.g.*, C, O, N and B [1,2]. To date, COFs have shown prospects in diverse areas, *e.g.*, gas adsorption and separation [3,4], heterogeneous catalysis [5–7], energy storage [8,9], sensors [10,11], drug delivery [12], and photoelectronics [13,14], thanks to their merits of high specific surface areas, ordered pore channels, facile structural and function design, *etc.* [15,16]. Recently, COFs have demonstrated as a promising platform to design high-performance heterogeneous photocatalysts for various chemical transformations [17], *e.g.*, photocatalytic water splitting [18,39], CO_2 reduction [19], organic conversion [5-7,40] and degradation of pollutants [20]. However, thus far, COFs as catalysts were attempted only in a few types of reactions. Therefore, it is desired to explore the potential of COFs to catalyze other kind of reactions, through for instance, delicate structural design.

Aryl boronic acids/esters as key reaction substrates are widely used in C-C bond formation by Suzuki coupling and can also be used to form C-N, C-O and C-S bonds [21,22]. In addition, they were applied to construct boronic ester and boroxine-linked COFs [23,24], develop luminescent materials [25], directly function as therapeutic agents and biological probes [26], *etc*. Commonly, aryl boronic acids/esters are readily prepared from aryl halides by using Grignard/organic lithium reagents or transition-metal catalysts or small-molecule-based photocatalysts [27]. Unfortunately, these methods still suffer from drawbacks, such as the high flammability of organic lithium reagents, toxicity of transition metals and non-recyclability of the catalysts. In addition, aryl boronic esters could also be produced by photocatalytic C-H borylation [28], obtained from aryldiazonium salts/amines [29], aryl mesylate/tosylate [30], and so on, which are interesting approaches but are much less frequently utilized than the aryl halides. In this respect, it is worthwhile developing an efficient metal-free and recyclable heterogeneous catalyst to mediate the borylation of aryl halides, which to the best of our knowledge, has yet been reported.

On account of the advantages of COFs to develop heterogeneous catalysts, in this work, we designed and synthesized three pyrene-based, nitrogen-rich, and imine-linked COFs, namely 6N-COF, 4N-COF and 2N-COF (Scheme 1), which were differentiated by the different number of N atoms in the building blocks of the COFs. The structural design principles include: (1) Pyrene-based and imine-linked COFs are well established and studied, exhibiting good stability and abundant visible-light absorption [31]; (2) Introducing nitrogen-containing heterocycles tailors the crystal packings and the electronic properties of the COFs, *e.g.*, the light absorption range and energy levels [32]. In addition, the reported heterocycle-free COF (0N-COF) was synthesized as well for comparison [36]. These COFs were attempted to mediate the borylation of aryl io-

* Corresponding authors.
E-mail addresses: liujunji@tju.edu.cn (J. Liu), gzhdream@live.com (G. Zhang), longchen@jlu.edu.cn (L. Chen).
[1] These authors contributed equally to this work.

https://doi.org/10.1016/j.cclet.2022.06.007
1001-8417/

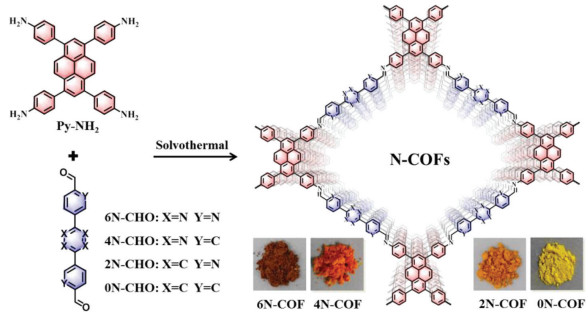

Scheme 1. Synthetic routes for the targeted N-COFs, *i.e.*, 6N-COF, 4N-COF, 2N-COF and 0N-COF.

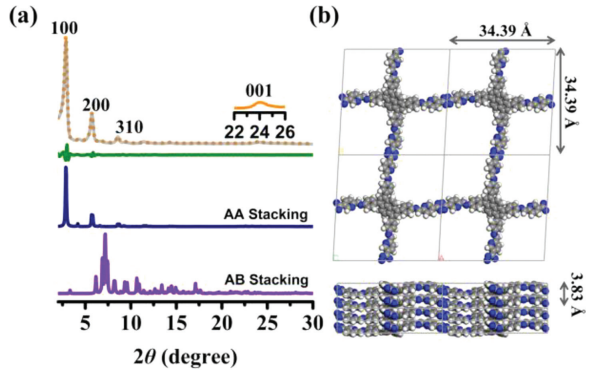

Fig. 1. (a) Experimentally observed PXRD pattern of 6N-COF (orange), Pawley-refined pattern (gray), difference between the experimental and calculated data (olive), and calculated patterns for AA (navy) and AB (violet) stacking. (b) Top and side views of the AA eclipsed stacking models of 6N-COF.

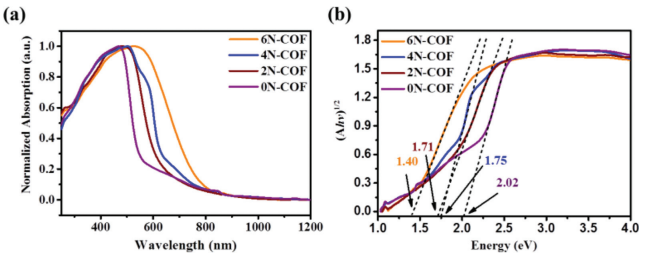

Fig. 2. (a) UV-vis absorption spectra and (b) Tauc plot of 6N-COF (orange), 4N-COF (blue), 2N-COF (dark red) and 0N-COF (violet) obtained with Kubelka-Munk function.

dides under visible light irradiation. It showed 6N-COF exhibited excellent photocatalytic performance among the others and also displayed excellent recyclability. This work demonstrates that COF as photocatalyst could successfully procure the borylation of aryl halides.

The targeted COFs were prepared by solvothermal method. Typically, 4,4′,4″,4‴-(1,3,6,8-pyrenetetrayl)tetraaniline (Py-NH_2) and the dialdehyde (Scheme 1), *i.e.*, 5,5′-(1,2,4,5-tetrazine-3,6-diyl)dipicolinaldehyde (6N-CHO) or 4,4′-(1,2,4,5-tetrazine-3,6-diyl)dibenzaldehyde (4N-CHO) or 5,5′-(1,4-phenylene)di(2-pyridinecarbaldehyde) (2N-CHO) or (1,1′:4′,1″-terphenyl)-4,4″-dicarbaldehyde (0N-CHO) were mixed together and heated under specific solvents at 120 °C for 3 days to form the targeted N-COFs (Supporting information for detailed procedures).

The chemical structures and compositions of N-COFs were characterized by Fourier transform infrared (FT-IR) spectroscopy, ^{13}C cross polarization total suppression of spinning sidebands (CP/TOSS) nuclear magnetic resonance (NMR) spectroscopy and elemental analysis. The FT-IR spectra of N-COFs (Fig. S7 in Supporting information) showed the signals of N-H stretching vibrations (3434-3211 cm^{-1}) and the C=O stretching modes (1719-1695 cm^{-1}) existing in the monomers were significantly attenuated in the corresponding COFs. At the same time, the peaks corresponding to the C=N stretching vibrations of the imine segments appeared in N-COFs in contrast to the monomers. Therefore, it suggests high degrees of polymerization have occurred during the synthesis of all N-COFs. In addition, the ^{13}C CP/TOSS NMR spectra of the 6N-COF, 4N-COF and 2N-COF displayed a notable peak at 158, 156 and 154 ppm respectively (Fig. S6 in Supporting information), which corresponded to the C signals of the imine linkages. Moreover, elemental analysis indicated the contents of C, H and N of N-COFs matched well with the theoretical values (Table S1 in Supporting information).

The crystalline structures of the as-synthesized N-COFs were characterized by powder X-ray diffraction (PXRD) analysis together with structural simulations. As shown in Fig. 1 and Fig. S23 (Supporting information), the PXRD spectra of 6N-COF displayed a prominent diffraction peak at 2.87° and three distnct signals at 5.61°, 8.59° and 23.34°, which were in accordance with the (100), (200), (310) and (001) facets, respectively. Similarly, the PXRD spectra of 4N-COF exhibited four notable peaks as well at 2.80°, 5.62°, 8.43° and 23.89°, which corresponded to the (100), (020), (300) and (001) facets, respectively. For 2N-COF, the diffraction signals appeared at 2.81°, 5.66°, 8.44° and 23.35°, which reflected the (100), (020), (310) and (001) facets, respectively. Geometric energy minimization and Pawley refinement were performed to determine the stacking modes, which revealed the simulated AA stacking rather than the staggered AB stacking of the targeted COFs correlated well with the experimental PXRDs. The optimized unit cell parameters for the targeted COFs are as follows: $a = b = 32.39$ Å, $c = 3.83$ Å, $\alpha = \beta = 90°$, $\gamma = 87°$ for 6N-COF with $R_{wp} = 5.63\%$ and $R_p = 3.98\%$; $a = b = 32.53$ Å, $c = 3.84$ Å, $\alpha = \beta = 90°$, $\gamma = 88°$ for 4N-COF with $R_{wp} = 4.51\%$ and $R_p = 2.81\%$; and $a = b = 32.58$ Å, $c = 3.78$ Å, $\alpha = \beta = 90°$, $\gamma = 86°$ for 2N-COF with $R_{wp} = 3.26\%$ and $R_p = 2.47\%$.

The morphologies of the as-synthesized COFs were characterized by scanning electron microscopy (SEM) and transmission electron microscopy (TEM). Both SEM and TEM images manifested all N-COFs exhibited aggregated block-shaped morphologies (Figs. S9-S12 in Supporting information). The thermal stabilities of these COFs were probed by thermogravimetric analysis (TGA) (Fig. S15 in Supporting information). It showed 6N-COF, 4N-COF, 2N-COF and 0N-COF could still maintain 90% of their initial weights up to 303 °C, 277 °C, 365 °C and 449 °C, respectively, which indicated good thermal stabilities of these COFs.

The porosities of the targeted COFs were evaluated by N_2 sorption and desorption measurements at 77 K. As depicted in Fig. S8 (Supporting information), the N_2 adsorption isotherms of 6N-COF, 4N-COF and 2N-COF exhibited typical type-IV isotherms, which indicated their mesoporous properties. From the N_2 adsorption isotherms, the Brunauer-Emmett-Teller (BET) surface areas of 6N-COF, 4N-COF and 2N-COF were calculated to be 1225, 1621 and 1798 m^2/g respectively. In addition, the average pore sizes of 6N-COF, 4N-COF and 2N-COF were calculated to be 3.10, 3.34 and 3.10 nm respectively, with the nonlocal density functional theory (NLDFT) method, which were consistent with the results calculated from PXRD data.

As shown in Fig. 2a, 0N-COF, 2N-COF, 4N-COF and 6N-COF displayed a broad light absorption, centered around 469, 493, 505 and 530 nm respectively, which were probably due to the π-π^* transitions of the extended conjugations of N-COFs. The apparent red-shifted peak absorptions of 4N-COF and 6N-COF, compared with those of 0N-COF and 2N-COF were consistent with the calculated much higher planarity of the building blocks of

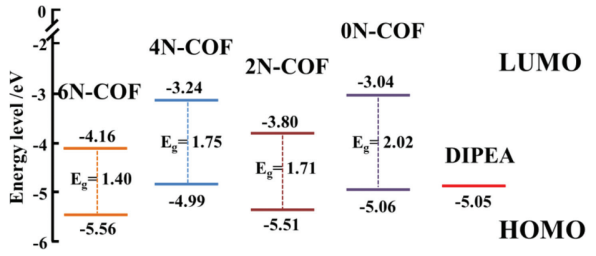

Fig. 3. Calculated HOMO and LUMO levels of 6N-COF (orange), 4N-COF (blue), 2N-COF (brownish red), 0N-COF (purple) and DIPEA (red).

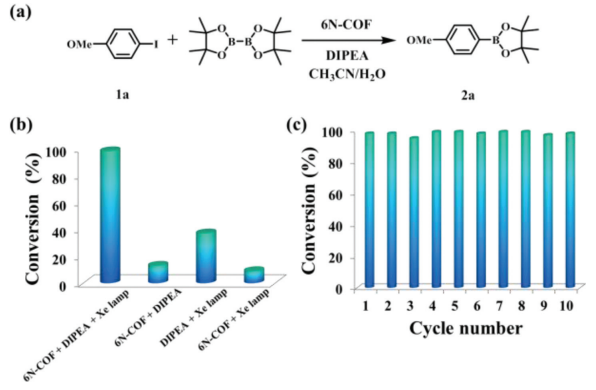

Fig. 4. (a) Borylation of 4-iodo-anisole. (b) Control experiments for borylation of 4-iodo-anisole under different conditions. (c) Assessment of the reusability of 6N-COF for the borylation of 4-iodo-anisole.

Table 1
Substrate scope of the borylation of aryl iodide under visible light irradiation.

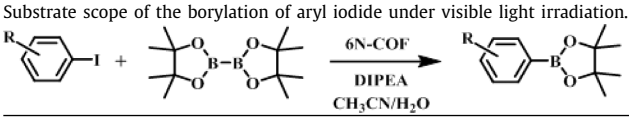

Entry	Substrate	Time (h)	Conversion (%)
1	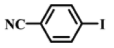	8	98
2	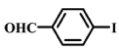	8	96
3	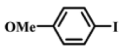	3.5	98
4	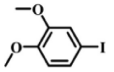	9.5	86
5	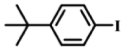	5	99
6	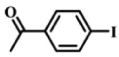	6	83
7	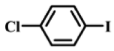	6	98
8		14	76
9		14	87

6N-COF and 4N-COF than those of 0N-COF, and 2N-COF (Fig. S24 in Supporting information). In general, N-COFs show notable absorptions covering the whole visible light region and the optical band gaps (E_g) of 0N-COF, 2N-COF, 4N-COF and 6N-COF were 2.02, 1.71, 1.75 and 1.40 eV, respectively, deduced from their absorption edges (Fig. 2b). Furthermore, cyclic voltammetry (CV) was performed to study the electrochemical properties of N-COFs with three-electrode system. As shown in Fig. S13 (Supporting information), the N-COFs displayed redox-active properties with notable oxidation and reduction peaks. The highest occupied molecular orbitals (HOMOs) of 6N-COF, 4N-COF, 2N-COF and 0N-COF were calculated to be −5.56, −4.99, −5.51 and −5.06 eV, respectively by comparing their oxidation onsets with that of ferrocene [37]. As shown in Fig. 3, the HOMO levels of N-COFs are close to that of *N*,*N*-diisopropylethylamine (DIPEA, a typical sacrificial reagent in photocatalytic reactions, Fig. S14a in Supporting information), which could facilitate the charge transport between the N-COFs and DIPEA during photocatalytic process [34,35].

Considering the nitrogen-rich architectures, high surface areas, broad light absorption and good stabilities of the targeted COFs, these COFs as the photocatalysts were attempted to mediate the borylation of aryl iodides into aryl boronic esters [38]. Taking 6N-COF as the model and 4-iodo-anisole and bis(pinacolato) boron as the substrates, we initially evaluated the catalytic performance of 6N-COF (Fig. 4a). As shown in Fig. 4b, we evaluated the influences of the catalyst, the sacrificial reagent—DIPEA and the light on the conversion efficiency of 4-iodo-anisole into 4-methoxybenzeneboronic acid pinacol ester. It showed the conversion of the reaction was up to 98% after reacting for 3.5 h, when 6N-COF, DIPEA and visible light (≥400 nm) were all applied. Keeping other conditions constant, however, the conversion was reduced to only 13% without light, 9% without DIPEA and 37% without 6N-COF. Therefore, it infers that the catalyst, sacrificial reagent and light radiation are all indispensable factors to render high conversions of this reaction. Furthermore, we investigated the catalytic performances of the other COFs, *i.e.*, 4N-COF, 2N-COF and 0N-COF at the same conditions as those for 6N-COF; it showed the conversion reached 88%, 44% and 21% for 2N-COF, 0N-COF and 4N-COF respectively (Table S2 in Supporting information). Consequently, it indicates 6N-COF outperforms the other three COFs as the photocatalyst for the borylation of aryl iodide under the same conditions. The better performance of 6N-COF could be attributed to several reasons, *e.g.*, broad light absorption, high surface area, and the proper energy level to render effective charge transfer during the reaction of 6N-COF.

To evaluate the applicability of 6N-COF as photocatalyst to promote the borylation of diverse aryl iodides, different aryl iodides were tested for the reaction. As shown in Table 1, the catalytic conversion efficiencies are quite high (≥76%) for both aryl iodides containing electron withdrawing groups (*e.g.*, cyano, chloro, and formyl) and aryl iodides incorporating electron-donating groups (*e.g.*, methoxy, alkyl). Therefore, it seems 6N-COF could effectively catalyze the borylation reaction in a broad substrate scope.

To evaluate the recyclability of 6N-COF as the photocatalyst, the recycling experiments were performed. After each test, 6N-COF could be easily recovered by centrifuge and subsequent washing with acetonitrile. As depicted in Fig. 4c, the conversion of the product could still reach 98% after 10 cycles, which suggested high recyclability of 6N-COF as a photocatalyst.

To investigate the photocatalytic mechanism of these N-COFs, we performed the electron paramagnetic resonance (EPR) measurement for the mixture of the 6N-COF, DIPEA in CH_3CN/H_2O solution after visible-light irradiation for 30 min. As shown in Fig. S16a (Supporting information), EPR spectra indicated a sextet (marked with stars) and a roughly quartet peak signals (marked with triangles), which revealed the existence of carbon and nitrogen centered radicals respectively [33]. In addition, a notable small peak (~21 ppm) appeared in the ^{11}B NMR spectra of the mixture of bis(pinacolato) boron and DIPEA, corresponding to the hydroxy-substituted bis(pinacolato) boron anion intermediate **1** (Figs. S16b

and S22 in Supporting information); however, this peak was minimal in the ^{11}B NMR spectra of bare bis(pinacolato) boron or the mixture of bis(pinacolato) boron and 4-iodo-anisole; it suggested the interaction between bis(pinacolato) boron and DIPEA promoted the formation of intermediate **1** [34].

Based on the above experiments and the previous reports [34,35], we proposed a probable photocatalytic mechanism of our COFs to mediate the borylation of aryl iodides (Fig. S22). On the one hand, treatment of bis(pinacolato) boron (**B**) with water in the presence of DIPEA leads to hydroxy-substituted bis(pinacolato) boron anion (**1**) and **2** ($DIPEAH^+$). On the other hand, irradiation of photocatalyst COF with xenon lamp provides an excited COF^* intermediate, and then a single-electron transfer of DIPEA to COF^* affords the $COF^{\bullet-}$ radical anion and $DIPEA^{\bullet+}$ radical cation. After that, electron transfer between $COF^{\bullet-}$ and aryl halide (**A**) forms aryl halide radical ainon **4** and regenerates COF for the next catalytic cycle. Then, elimination of halogen anion (X^-) from radical anion **4** gives aryl radical **5** which subsequently reacts with **1** to generate aryl boronic ester radical anion **7**. Finally, electron transfer between **7** and $DIPEA^{\bullet+}$ produces the aryl boronic ester (**C**).

In conclusion, three new pyrene-based, nitrogen-rich and imine-linked 2D COFs were successfully prepared. These COFs exhibited excellent crystallinity, high specific surface areas, broad light absorption and redox-active properties. Interestingly, these COFs demonstrate their capability as photocatalysts to mediate the borylation of aryl iodides, which to the best of our knowledge, represent the first examples of COF catalysts for the borylation of aryl halides. In addition, 6N-COF outperformed the other three COFs in the photocatalytic performance, which could be attributed to its proper energy levels, broader light absorption and high specific surface area. This work expands the COF-catalyzed reaction scopes and provides insights into designing high-performance COF-based photocataylsts.

Declaration of competing interest

The authors declare that they have no known competing financial interests or personal relationships that could have appeared to influence the work reported in this paper.

Acknowledgment

This work was financially supported by National Natural Science Foundation of China (No. 51973153).

Supplementary materials

Supplementary material associated with this article can be found, in the online version, at doi:10.1016/j.cclet.2022.06.007.

References

[1] A.P. Côté, A.I. Benin, N.W. Ockwig, et al., Science 310 (2005) 1166–1170.
[2] S.Y. Ding, W. Wang, Chem. Soc. Rev. 42 (2013) 548–568.
[3] Z. Wang, S. Zhang, Y. Chen, Z. Zhang, S. Ma, Chem. Soc. Rev. 49 (2020) 708–735.
[4] S.S. Han, H. Furukawa, O.M. Yaghi, W.A. Goddard, J. Am. Chem. Soc. 130 (2008) 11580–11581.
[5] X. Yan, H. Liu, Y. Li, et al., Macromolecules 52 (2019) 7977–7983.
[6] K. Zhang, G. Lu, Z. Xi, Chin. Chem. Lett. 32 (2021) 2207–2211.
[7] W. Hao, D. Chen, Y. Li, et al., Chem. Mater. 31 (2019) 8100–8105.
[8] M. Li, J. Liu, Y. Li, et al., CCS Chem. 2 (2020) 696–706.
[9] J. Li, X. Jing, Q. Li, et al., Chem. Soc. Rev. 49 (2020) 3565–3604.
[10] W.K. Haug, E.M. Moscarello, E.R. Wolfson, P.L. McGrier, Chem. Soc. Rev. 49 (2020) 839–864.
[11] H. Qi, B. Liang, U. Kaiser, SmartMat 2 (2021) 131–138.
[12] Q. Fang, J. Wang, S. Gu, et al., J. Am. Chem. Soc. 137 (2015) 8352–8355.
[13] Y. Lv, Y. Li, G. Zhang, et al., CCS Chem. 3 (2021) 1773–1779.
[14] X. Yan, S. Lyu, X. Xu, et al., Angew. Chem. Int. Ed. (2022) e202201900.
[15] M.S. Lohse, T. Bein, Adv. Funct. Mater. 28 (2018) 1705553.
[16] T.F. Machado, M.E.S. Serra, D. Murtinho, A.J.M. Valente, M. Naushad, Polymers 13 (2021) 970–1007.
[17] S. Ding, J. Gao, Q. Wang, et al., J. Am. Chem. Soc. 133 (2011) 19816–19822.
[18] D. Mullangi, V. Dhavale, S. Shalini, et al., Adv. Energy Mater. 6 (2016) 1600110.
[19] R.K. Yadav, A. Kumar, N.J. Park, K.J. Kong, J.O. Baeg, J. Mater. Chem. A 4 (2016) 9413–9418.
[20] Y. Tang, W. Li, Y. Muhammad, et al., Chem. Eng. J. 421 (2021) 129743.
[21] U. Solmaz, I. Gumus, M.K. Yilmaz, S. Ince, H. Arslan, Appl. Organomet. Chem. 35 (2021) 6348–6364.
[22] L. Chen, J. Yang, P. Xu, et al., J. Org. Chem. 85 (2020) 7515–7525.
[23] C. Li, Y. Wang, Y. Zou, et al., Angew. Chem. Int. Ed. 59 (2020) 9403–9407.
[24] D.J. Rizzo, Q. Dai, C. Bronner, et al., Nano Lett. 20 (2020) 963–970.
[25] Y. Shoji, Y. Ikabata, Q. Wang, et al., J. Am. Chem. Soc. 139 (2017) 2728–2733.
[26] B. Das, P. Thapa, R. Karki, et al., Future Med. Chem. 5 (2013) 653–676.
[27] B. Yadagiri, K. Daipule, S.P. Singh, Asian J. Org. Chem. 10 (2021) 7–37.
[28] I.A.I. Mkhalid, J.H. Barnard, T.B. Marder, J.M. Murphy, J.F. Hartwig, Chem. Rev. 110 (2010) 890–931.
[29] F. Mo, G. Dong, Y. Zhang, J. Wang, Org. Biomol. Chem. 11 (2013) 1582–1593.
[30] D.A. Wilson, C.J. Wilson, C. Moldoveanu, et al., J. Am. Chem. Soc. 132 (2010) 1800–1801.
[31] Z. Almansaf, J. Hu, F. Zanca, et al., ACS Appl. Mater. Interfaces 13 (2021) 6349–6358.
[32] W. Wu, Q. Zhang, X. Wang, et al., ACS Catal. 7 (2017) 7267–7273.
[33] M. Jiang, H. Yang, H. Fu, Org. Lett. 18 (2016) 5248–5251.
[34] J.C. Herrera-Luna, D. Sampedro, M. Consuelo Jimenez, R Pe ŕez Ruiz, Org. Lett. 22 (2020) 3273–3278.
[35] K. Chen, S. Zhang, P. He, P. Li, Chem. Sci. 7 (2016) 3676–3680.
[36] N. Huang, P. Wang, M.A. Addicoat, T. Heine, D. Jiang, Angew. Chem. Int. Ed. 56 (2017) 4982–4986.
[37] D. Chen, W. Chen, G. Zhang, et al., ACS Catal. 12 (2022) 616–623.
[38] L. Zhang, L. Jiao, J. Am. Chem. Soc. 141 (2019) 9124–9128.
[39] R. Chen, Y. Wang, Y. Ma, et al., Nat. Commun. 12 (2021) 1354.
[40] R. Chen, J. Shi, Y. Ma, et al., Angew. Chem. Int. Ed. 58 (2019) 6430–6434.